Available online at www.sciencedirect.com

SciVerse ScienceDirect

Ceramics International 38 (2012) 1365–1370

CERAMICS INTERNATIONAL

www.elsevier.com/locate/ceramint

Sm^{3+}-doped $CaTiO_3$ phosphor: Synthesis, structure, and photoluminescent properties

Myoung Gyu Ha [a], Mi Rang Byeon [a], Tae Eun Hong [a,b], Jong Seong Bae [a], Yangsoo Kim [c], S. Park [b], Ho-Soon Yang [b,**], K.S. Hong [a,*]

[a] Pusan Center, Korea Basic Science Institute, Pusan 618-230, Republic of Korea
[b] Department of Physics, Pusan National University, Pusan 609-735, Republic of Korea
[c] Sunchon Center, Korea Basic Science Institute, Sunchon 540-742, Republic of Korea

Received 29 March 2011; received in revised form 5 September 2011; accepted 6 September 2011
Available online 14 September 2011

Abstract

Photoluminescent properties of samarium-doped calcium titanate for near ultra-violet excitation were studied. $CaTiO_3:Sm^{3+}$ phosphor was synthesized by using the solid-state reaction method. The structure and properties of the phosphor were characterized by using X-ray diffractometer, scanning electron microscope, UV–visible spectrophotometer, high-resolution secondary ion mass spectrometer, and X-ray photoelectron spectrometer. The photoluminescent properties were studied by taking excitation and emission spectra. A strong red–orange luminescence corresponding to $^4G_{5/2} \rightarrow {}^6H_{7/2}$ transition of Sm^{3+} for near ultra-violet excitation was observed. It was found that $CaTiO_3:Sm^{3+}$ was a red–orange emitting phosphor and had higher efficiency for the operation with near ultra-violet excitation.

Keywords: $CaTiO_3$; Sm^{3+}; Solid state reaction; Red–orange emission; Near ultraviolet excitation

1. Introduction

Rare-earth ions-doped materials have been studied extensively because they can be applied to plasma display panels, field emission displays, light-emitting diodes (LEDs), cathode ray tubes, and optoelectronic devices [1–3]. Recently, rare-earth ions-doped titanates have attracted lots of attention because of their promising luminescent properties and potential applications to white LEDs [4]. Rare-earth ions-doped calcium titanate ($CaTiO_3$) phosphors have been studied extensively due to the well-known chemical stability which can be used as LEDs [4–6].

We have reported highly efficient red-emission in $CaTiO_3:Eu^{3+}$ phosphors for near ultra-violet (NUV) excitation in our previous work [7]. Since trivalent samarium (Sm^{3+}) has been known to exhibit a strong emission in red–orange region [3,8–13] for the application of full color displaying devices [4], the current work focused on Sm^{3+}-doped $CaTiO_3$ phosphors.

In this work, we synthesized $CaTiO_3:Sm^{3+}$ phosphors by using the solid-state reaction method in order to find the possibility of the applications as rare-earth ions-doped phosphors for NUV excitation. We characterized the structures and properties of $CaTiO_3:Sm^{3+}$ phosphors. We studied photoluminescent properties of $CaTiO_3:Sm^{3+}$ phosphors by taking excitation and emission spectra at room temperature. We found that the $CaTiO_3:Sm^{3+}$ phosphors were red-emitting phosphors and had higher efficiency for the operation with the NUV excitation.

2. Experimental details

$CaTiO_3:Sm^{3+}$ phosphors were synthesized by using the solid state reaction method. The starting materials were calcium carbonate ($CaCO_3$, Aldrich, 99.0%), titanium dioxide (TiO_2, Aldrich, 99.8%), and samarium oxide (Sm_2O_3, Aldrich, 99.9%). In our pre-experiments, we have changed the amounts of TiO_2 and Sm_2O_3 together. But we could not observe any other phase except [$CaTiO_3$] in X-ray diffraction measurement

* Corresponding author. Tel.: +82 51 974 6106.
** Corresponding author. Tel.: +82 51 510 2221.
E-mail addresses: hsyang@pusan.ac.kr (H.-S. Yang), kyongsoo@kbsi.re.kr (K.S. Hong).

0272-8842/$36.00
doi:10.1016/j.ceramint.2011.09.015

regardless of the doped amount of samarium. Thus we kept the mole ratio of $CaCO_3$ and TiO_2 as 1:1 during the sample preparation process. The concentrations of Sm^{3+} ions were varied from 0.1 mole% to 7.0 mole% while the amount of $CaCO_3$ and TiO_2 were fixed to 1 mole in all samples. The materials were ball-milled thoroughly in ethanol for 24 h for homogeneous mixing of small amount of activators. They were dried at 100 °C for 24 h and sintered at 1300 °C for 4 h in atmosphere. The materials were cooled down to room temperature and then crushed into a fine powder. The synthesized powders were characterized by using the conventional X-ray diffractometer (XRD, Rigaku D-2400), scanning electron microscope (SEM, Coxem CX-100S), high-resolution secondary ion mass spectrometer (Nano-SIMS, Cameca NS50), and X-ray photoelectron spectrometer (XPS, Escalab 250).

The Nano-SIMS analysis was performed by using cesium primary ion beam with a diameter 100 nm, impact energy 16.0 keV, and a beam current 1.5 pA in order to obtain the optimized acquisition images. The raster size was 30 μm × 30 μm in all images and stepped over the sample in 256 pixels × 256 pixels to generate qualitative secondary ion images. The counting time was 10 ms/pixel. Samples were also simultaneously imaged using the secondary ions that were detected by an electron multiplier.

The synthesized powder was pressed into a pellet for the absorption and photoluminescence (PL) measurements. Absorption spectra were taken by using UV–visible spectrophotometer (Varian Cary300). PL spectra were taken with a steady-state fluorescence system with a 450 W Xe-lamp. The excitation light from the Xe-lamp (Muller Electronik-Optik LAX-1000) selected by using a 300 mm focal length monochromator (Dongwoo DM320i) was focused onto the sample. Fluorescence from the sample was collimated and refocused into the emission monochromator (Dongwoo DM320i) with a 300 mm focal length. PL was detected by using a photomultiplier tube (PMT, Hamamatsu R955) after passing the cut-off filter (Edmund OG 515) and was accumulated with a computer. All spectra were taken at room temperature.

3. Results and discussion

We have tried several temperatures with different sintering times to obtain the best crystallization conditions for crystallization of the phosphors at a fixed Sm^{3+} concentration. From XRD and PL measurements of the synthesized samples, we found that the best sintering conditions for our $CaTiO_3$:Sm^{3+} phosphors were 1300 °C and 4 h. Although the [$CaTiO_3$] phase and PL were observed at the samples prepared with different sintering conditions, the sample prepared with 1300 °C and 4 h showed the strongest PL intensity. Therefore we will focus on the samples prepared with these sintering conditions throughout the article.

Fig. 1 shows XRD patterns of $CaTiO_3$:Sm^{3+} phosphors of (a) 5.0 mole%, (b) 2.0 mole%, and (c) 0.1 mole%. The monoclinic-structured $CaTiO_3$ patterns from the JCPDS file [14] were shown as Fig. 1(d) for comparison. Monoclinic [$CaTiO_3$] phase was clearly observed at all samples having various concentrations of Sm^{3+} as shown in Fig. 1. The peaks were well resolved at low concentrations of Sm^{3+}, and getting broader and unresolvable (peaks at 33° and 59°) as the concentration increased because of the large ionic radii of Sm^{3+} ions. However, there was no change in the overall crystal structure as the concentration increased up to 7.0 mole%.

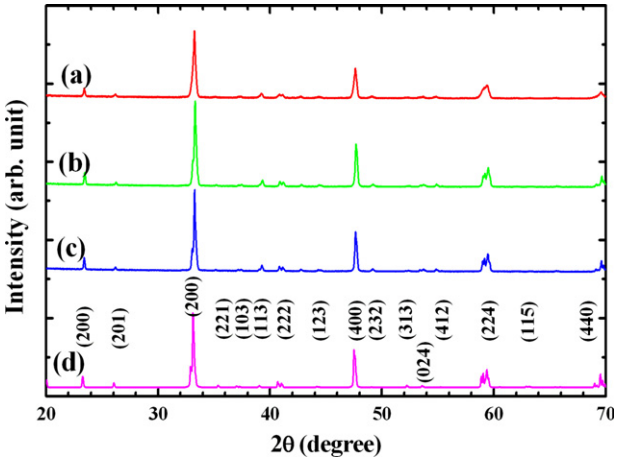

Fig. 1. XRD patterns of $CaTiO_3$:Sm^{3+} phosphors. Sm^{3+} concentrations are (a) 5.0 mole%, (b) 2.0 mole%, (c) 0.1 mole%, and (d) monoclinic-structured $CaTiO_3$. Upper patterns are shifted vertically for clarity.

Fig. 2 shows SEM images of $CaTiO_3$:Sm^{3+} phosphors of 2.0 mole%. We checked all phosphors and found uniform structure with grain size of a few micrometers. The obtained sizes of powders were close to the calculated values by using the Scherrer's equation and peaks of Fig. 1.

The Nano-SIMS is a powerful tool in elemental analysis by tracing a small amount of elements and isotopes at high spatial resolutions. The Nano-SIMS offers the possibility of imaging components based on the elemental or isotopic compositions of their atomic and molecular ion fragments with high lateral resolution and sensitivity, yielding information that can complement other analytical methods, including many other

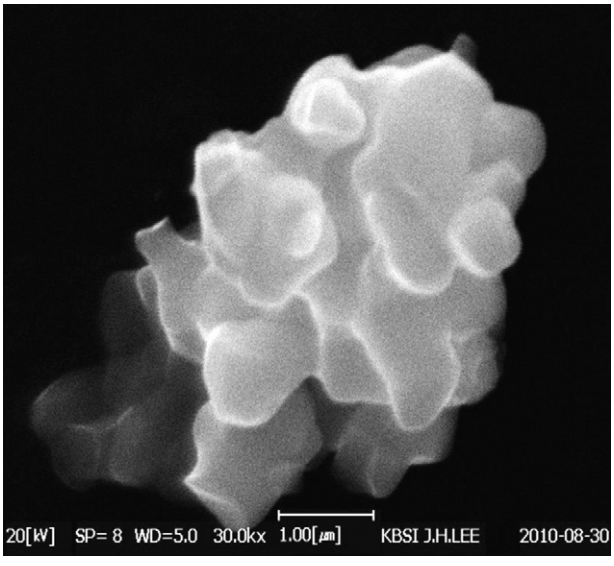

Fig. 2. SEM images of $CaTiO_3$:Sm^{3+} phosphor of 2.0 mole% concentration.

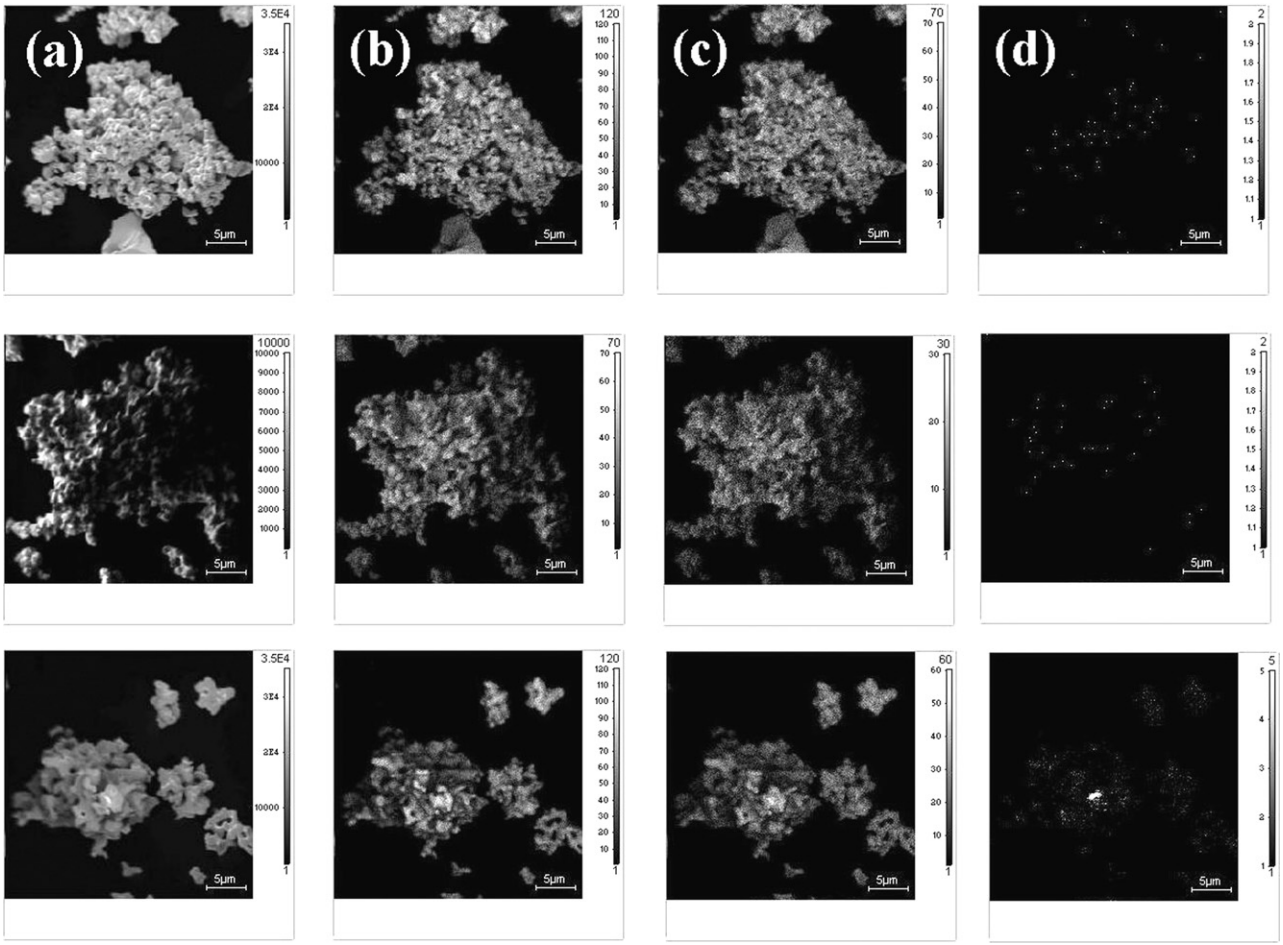

Fig. 3. Qualitative analysis for the elemental acquisition images of $CaTiO_3$:Sm^{3+} (a) oxygen, (b) calcium, (c) titanium, and (d) samarium ions for Sm^{3+} concentrations of 0.3 mole% (top), 2.0 mole% (middle), and 7.0 mole% (bottom), respectively.

types of SIMS experiments [15]. Above all, the Nano-SIMS provides the capability of recording five atomic mass images together simultaneously with a high spatial resolution of 50 nm. These characteristics have made Nano-SIMS a standard tool for the materials study, and Nano-SIMS can compare elemental distributions exactly at a fixed position of the sample. Thus we used Nano-SIMS to study the element compositional analysis.

Fig. 3 shows the elemental acquisition images of (a) oxygen, (b) calcium, (c) titanium, and (d) samarium for the concentrations of 0.3 mole% (top), 2.0 mole% (middle), and 7.0 mole% (bottom), respectively. The elemental acquisition images were taken in high vacuum without etching the surface of the samples. The acquired elemental images showed that the elements were distributed throughout the samples. Since we could not obtain the reference samples, the obtained images provide only qualitative information of the elements. We could observe the existence of samarium even in the lower concentrations. As far as our knowledge is concerned, the acquisition images of doped rare earth ions in phosphors obtained by using the Nano-SIMS must be the first time to be reported. It means that the high lateral resolution of the Nano-SIMS provides a unique tool for the investigation of elements in materials.

In order to see the chemical states of titanium and the amount of doped samarium, we took XPS spectra of the synthesized phosphors. Fig. 4 shows wide scan XPS spectra of $CaTiO_3$:Sm^{3+} phosphors. Sm^{3+} concentrations are (a) 7.0 mole%, (b) 2.0 mole%, and (c) 0.3 mole%. The elements

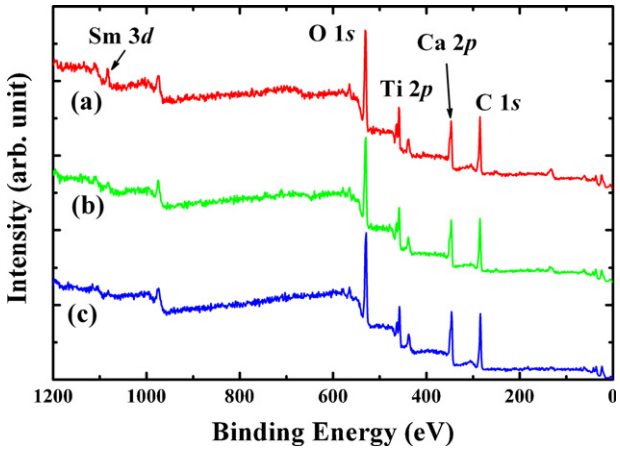

Fig. 4. Wide scan XPS spectra of $CaTiO_3$:Sm^{3+} phosphors. Sm^{3+} concentrations are (a) 7.0 mole%, (b) 2.0 mole%, and (c) 0.3 mole%. Upper spectra are shifted vertically for clarity.

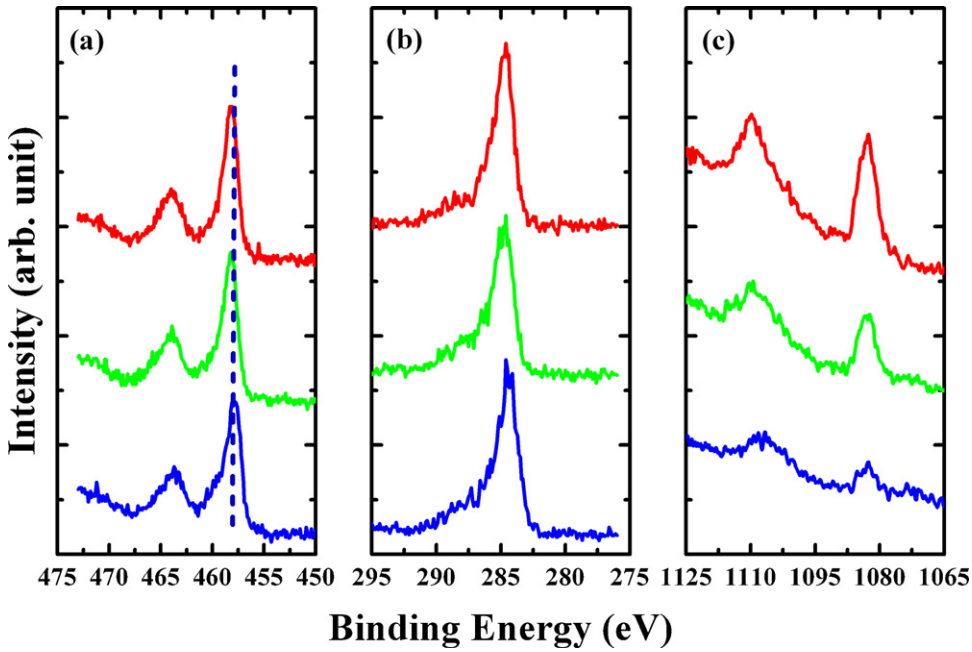

Fig. 5. Narrow scan XPS spectra of (a) titanium 2*p* states, (b) carbon 1*s* states, and (c) samarium 3*d* states in $CaTiO_3$:Sm^{3+} phosphors. Sm^{3+} concentrations are 7.0 mole%, 2.0 mole%, and 0.3 mole%, respectively, from top to bottom in all three figures. Upper spectra are shifted vertically for clarity.

such as C, Ca, Ti, O, and Sm were observed in measurement. When the starting materials were burned in atmosphere like our sintering process, most of the oxygen and carbon in the starting materials were consumed during sintering process inside the furnace. Since XPS spectra were taken in vacuum without etching the surface of the samples, the observed carbon peaks were considered due to the atmospheric carbon during the measurement preparations.

We took narrow scan XPS spectra to each element for better understanding. Fig. 5 shows narrow scan XPS spectra of (a) titanium 2*p* states, (b) carbon 1*s* states, and (c) samarium 3*d* states in $CaTiO_3$:Sm^{3+} phosphors. The Sm^{3+} concentrations are 7.0 mole%, 2.0 mole%, and 0.3 mole%, respectively, from top to bottom, in each figure. In Fig. 5(a), the peak positions for titanium 2*p* states (indicated by dotted line) were the same in the samples of different Sm^{3+} concentration. This means that the binding energy did not change regardless of the amount of doped Sm^{3+} concentrations. The observed binding energy determined that the chemical state of titanium ions was Ti^{4+} [16]. Fig. 5(b) shows the atmospheric carbon attached during the measurement preparation. Fig. 5(c) shows the variation of the doped amount of Sm^{3+} qualitatively in $CaTiO_3$:Sm^{3+} phosphors according to the concentrations.

Fig. 6 shows UV–visible absorption spectra of $CaTiO_3$:Sm^{3+} phosphors. The Sm^{3+} concentrations are (a) 5.0 mole%, (b) 3.0 mole%, and (c) 1.0 mole%. For the samples of lower concentrations such as 0.5 mole% and 0.1 mole%, the absorption was too weak to observe. In our previous work on $CaTiO_3$:Eu^{3+} phosphors [7], the absorption peak intensities were weak to observe for the concentrations of less than 1.0 mole%. A strong absorption band of NUV was observed around 408 nm corresponding to $^6H_{5/2} \rightarrow {}^4F_{7/2}$ from doped Sm^{3+} ions. Other observed absorption bands were identified to the electronic transitions such as $^6H_{5/2} \rightarrow {}^4D_{3/2}$ at 364 nm, $^6H_{5/2} \rightarrow {}^4D_{1/2}$ at 379 nm, $^6H_{5/2} \rightarrow ({}^6P,{}^4P)_{5/2}$ at 421 nm, $^6H_{5/2} \rightarrow {}^4G_{9/2}$ at 440 nm, $^6H_{5/2} \rightarrow {}^4I_{13/2}$ at 465 nm, and $^6H_{5/2} \rightarrow {}^4I_{11/2}$ at 481 nm [17]. Most of these bands were also observed in the excitation spectra which will be shown later. From these absorption bands, we understood that the luminescent properties were originated from the direct transitions from the ground state $^6H_{5/2}$ to the excited states of Sm^{3+}, not via the energy transfer processes [18,19].

Fig. 7 shows the excitation spectra monitored at 600.2 nm emission of $CaTiO_3$:Sm^{3+} phosphors. The Sm^{3+} concentrations are (a) 2.0 mole%, (b) 1.0 mole%, and (c) 0.3 mole%. The identified excitation bands were $^4D_{3/2}$ at 365 nm, $^4D_{1/2}$ at 379 nm, $^4F_{7/2}$ at 408 nm, $({}^6P,{}^4P)_{5/2}$ at 422 nm, $^4G_{9/2}$ at 441 nm, $^4I_{13/2}$ at 467 nm, and $^4I_{11/2}$ at 480 nm [17]. All these bands were

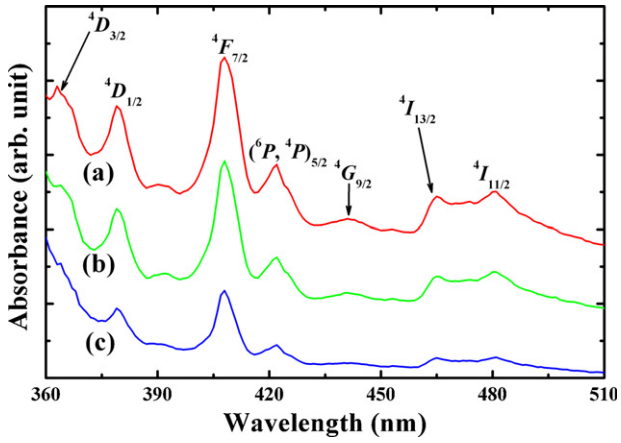

Fig. 6. UV–visible absorption spectra of $CaTiO_3$:Sm^{3+} phosphors. Sm^{3+} concentrations are (a) 5.0 mole%, (b) 3.0 mole%, and (c) 1.0 mole%. Upper spectra are shifted vertically for clarity.

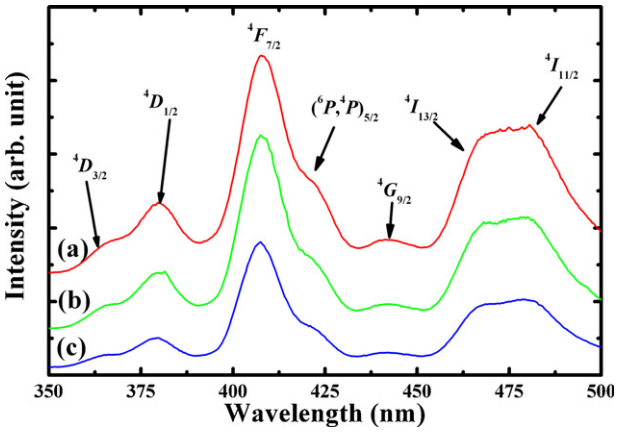

Fig. 7. Excitation spectra of $CaTiO_3:Sm^{3+}$ phosphors. Sm^{3+} concentrations are (a) 2.0 mole%, (b) 1.0 mole%, and (c) 0.3 mole%. Upper spectra are shifted vertically for clarity.

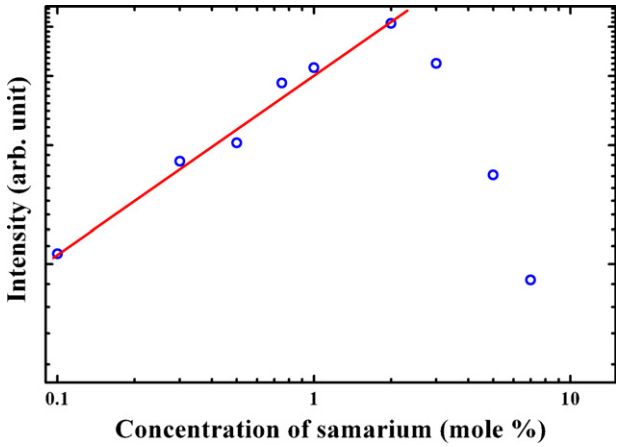

Fig. 9. Concentration dependent emission intensities corresponding to $^4G_{5/2} \rightarrow {}^6H_{7/2}$ transition of Sm^{3+} in $CaTiO_3:Sm^{3+}$ phosphors based on Fig. 8. The straight line is a least square fit to the lower concentration data points.

the transitions from the ground state, $^6H_{5/2}$, to the higher energy states of Sm^{3+}. Since the transition corresponding to $^6H_{5/2} \rightarrow {}^4F_{7/2}$ at 408 nm had the maximum intensity among these bands, the emission spectra were taken with the excitation from this band position. The transitions in these excitation spectra were closely correlated with those of absorption spectra in UV–visible region shown in Fig. 6.

Fig. 8 shows the emission spectra of $CaTiO_3:Sm^{3+}$ phosphors with the excitation of $^6H_{5/2} \rightarrow {}^4F_{7/2}$ at 408 nm. The Sm^{3+} concentrations are (a) 2.0 mole%, (b) 0.5 mole%, and (c) 0.1 mole%. The identified emission bands were by the intra 4*f* transitions of Sm^{3+} such as $^4G_{5/2} \rightarrow {}^6H_{5/2}$ at 565 nm, $^4G_{5/2} \rightarrow {}^6H_{7/2}$ at 600 nm, and $^4G_{5/2} \rightarrow {}^6H_{9/2}$ at 646 nm. Among these, the transition $^4G_{5/2} \rightarrow {}^6H_{7/2}$ has strongest intensity and this can be applied to the red–orange emitting display materials.

The transition $^4G_{5/2} \rightarrow {}^6H_{7/2}$ satisfies the selection rule of $\Delta J = \pm 1$, where J is the angular momentum. Magnetic dipole transitions obey the selection rule of $\Delta J = 0$ and ± 1, and electric dipole transitions obey the selection rule of $\Delta J \leq 6$ unless J or $J' = 0$ when $\Delta J = 2,3,6$ [13]. The transitions $^4G_{5/2} \rightarrow {}^6H_{5/2}$ and $^4G_{5/2} \rightarrow {}^6H_{7/2}$ are magnetic dipole transitions, while the transition $^4G_{5/2} \rightarrow {}^6H_{9/2}$ is an electric dipole transition.

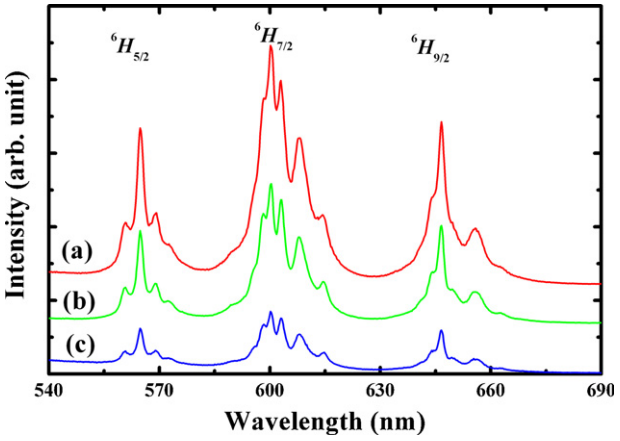

Fig. 8. Emission spectra of $CaTiO_3:Sm^{3+}$ phosphors. Sm^{3+} concentrations are (a) 2.0 mole%, (b) 0.5 mole%, and (c) 0.1 mole%. Upper spectra are shifted vertically for clarity.

Consider the ratio between the intensities of the electric dipole transition and magnetic dipole transition. The local symmetry is measured with the relative intensity of these two transitions. The larger value of this ratio means more distortion from the inversion symmetry [20]. The obtained values were kept almost constant between 1.40 for 0.5 mole% and 1.53 for 3.0 mole%, which meant that the Sm^{3+} ions were still embedded in the $CaTiO_3$ structures rather than in the distorted cation environment. In our previous result for $CaTiO_3:Eu^{3+}$ phosphors [7], the value varied from 1.77 to 3.11, which implied that the environment of Eu^{3+} ions were more distorted or asymmetric state. The structural change can be monitored with the spectral width [21]. There was no significant change in the observed spectral widths for the samples in Fig. 8. Therefore there was no change in the structural environment around Sm^{3+} ions with increase of the concentration, which means that the $CaTiO_3:Sm^{3+}$ phosphors can be a promising candidate for photonic applications.

Although we showed the emission spectra of three samples in Fig. 8, we could observe the same emission patterns in all synthesized samples. We plotted the intensities of the strongest emission peak of $CaTiO^3:Sm^{3+}$, $^4G_{5/2} \rightarrow {}^6H_{7/2}$, according to the Sm^{3+} concentrations in log–log scale as shown in Fig. 9. The straight line is a least square fit to the data points of lower concentration. PL intensity increased almost linearly as the concentration increased up to 2.0 mole% and then decreased. We found that the best concentration of $CaTiO_3:Sm^{3+}$ phosphor for display applications is about 2.0 mole% in our system. The quenching of PL intensity with the Sm^{3+} concentration was attributed to a decrease in the number of optically active Sm^{3+} ions. Since we took all the spectra at room temperature, we could not confirm whether this decrease was due to thermal phonons or not.

4. Summary

We synthesized $CaTiO_3:Sm^{3+}$ phosphors by using the solid state reaction method and characterized their properties by

using XRD, SEM, Nano-SIMS, XPS, and UV–visible spectrophotometer. We studied their photoluminescent properties caused by the chemical compositions in red–orange emitting phosphors. The luminescent features were obtained by analyzing the variations in the emission and excitation spectra with the concentrations. We found that the red–orange emitting $CaTiO_3:Sm^{3+}$ phosphors could be a promising candidate for photonic applications.

Acknowledgement

This work was supported by KBSI grant K3108A to J. P. Kim.

References

[1] B. Yan, X. Su, K. Zhou, In situ chemical coprecipatation composition of hybrid precursors to red $YVO_4:Eu^{3+}$ and green $LaPO_4:Tb^{3+}$ phosphors, Mater. Res. Bull. 41 (2006) 134–143.

[2] R. Stefani, A.D. Maia, E.E.S. Teotonio, M.A.F. Monteiro, M.C.F.C. Felinto, H.F. Brito, Photoluminescent behavior of $SrB_4O_7:RE^{2+}$ (RE = Sm and Eu) prepared by Pechini, combustion and ceramic methods, J. Solid State Chem. 179 (2006) 1086–1092.

[3] G.S.R. Raju, S. Buddhudu, Photoluminescence analysis of Sm^{3+} and Dy^{3+} doped PVA films, J. Appl. Polym. Sci. 107 (2008) 2480–2485.

[4] X.M. Liu, P.Y. Jia, J. Liu, Monodisperse spherical core–shell structured SiO_2–$CaTiO_3:Pr^{3+}$ phosphors for field emission displays, J. Appl. Phys. 99 (2006) 124902.

[5] J.S. Kim, P.E. Jeon, J.C. Choi, H.L. Park, S.I. Mho, C.G. Kim, Warm-white-light emitting diode utilizing a single-phase full-color $Ba_3MgSi_2O_8:Eu^{2+}$, Mn^{2+} phosphor, Appl. Phys. Lett. 84 (2004) 2931–2933.

[6] P.J. Deren, R. Pazik, W. Strek, Ph. Boutinaud, R. Mahiou, Synthesis and spectroscopic properties of $CaTiO_3$ nanocrystals doped with Pr^{3+} ions, J. Alloys Compd. 451 (2008) 595–599.

[7] M.G. Ha, J.H. Lee, J.S. Bae, J.P. Kim, E.D. Jeong, K.S. Hong, H.S. Yang, Photophysical properties of highly efficient red-emitting $CaTiO_3:Eu^{3+}$ phosphors under near ultra-violet excitation, Curr. Appl. Phys. 11 (2011) 1379–1383.

[8] G. Lakshminarayana, S. Buddhudu, Spectral analysis of Sm^{3+} and Dy^{3+}: B_2O_3–ZnO–PbO glasses, Physica B 373 (2006) 100–106.

[9] V.S. Marques, L.S. Cavalcante, J.C. Sczancoski, E.C. Paris, J.M.C. Teixeira, J.A. Varela, F.S. De Vicente, M.R. Joya, P.S. Pizani, M.S. Li, M.R.M.C. Santos, E. Longo, Synthesis of (Ca,Nd)TiO_3 powders by complex polymerization, Rietveld refinement and optical properties, Spectrochim. Acta A 74 (2009) 1050–1059.

[10] Y. Zhang, R. Pang, C. Li, C. Zang, Q. Su, Reddish orange long lasting phosphorescence of Sm^{3+} in $Sr_2ZnSi_2O_7:Sm^{3+}$ phosphors, J. Rare Earths 28 (2010) 705–708.

[11] S.K.L. Devi, K. Sudarsanakumar, Photoluminescent properties of Sm^{3+}-doped zinc oxide nanostructures, J. Lumin. 130 (2010) 1221–1224.

[12] S.S. Sundari, K. Marimuthu, M. Sivraman, S.S. Babu, Composition dependent structural and optical properties of Sm^{3+}-doped sodium borate and sodium fluoroborate glasses, J. Lumin. 130 (2010) 1313–1319.

[13] Z. Cui, R. Ye, D. Deng, Y. Hua, S. Zhao, G. Jia, C. Li, S. Xu, Eu^{2+}/Sm^{3+} ions co-doped white light luminescence $SrSiO_3$ glass-ceramics phosphor for White LED, J. Alloys Compd. 509 (2011) 3553–3558.

[14] Inorganic Crystal Structure Database (http://http://icsd.fiz-karlsruhe.de).

[15] M.L. Kraft, S.F. Fishel, C.G. Marxer, P.K. Weber, I.D. Hutcheon, S.G. Boxer, Quantitative analysis of supported membrane composition using the NanoSIMS, Appl. Surf. Sci. 252 (2006) 6950–6956.

[16] J.F. Moulder, W.F. Stickle, P.E. Sobol, K.D. Bomben, in: J. Chastain, R.C. King, Jr. (Eds.), Handbook of X-ray Photoelectron Spectroscopy, Physical Electronics Inc., Minnesota, 1995.

[17] W.T. Carnall, H. Crosswhite, H.M. Crosswhite, Argonne Report ANL-78-95 (1978).

[18] X. Gao, L. Lei, C. Lv, Y. Sun, H. Zheng, Y. Cui, Preparation and photoluminescence property of a loose powder, $Ca_3Al_2O_6:Eu^{3+}$ by calcination of a layered double hydroxide precursor, J. Solid State Chem. 181 (2008) 1776–1781.

[19] H. Zhang, X. Fu, S. Niu, Q. Xin, Synthesis and photoluminescence properties of Eu^{3+}-doped $AZrO_3$ (A = Ca, Sr, Ba) perovskite, J. Alloys Compd. 459 (2008) 103–106.

[20] R.K. Brow, D.R. Tallant, G.L. Turner, Raman and 11B Nuclear magnetic resonance spectroscopic studies of alkaline-earth lanthanoborate glasses, J. Am. Ceram. Soc. 79 (1996) 2410–2416.

[21] B. Henderson, G.F. Imbusch, Optical Spectroscopy of Inorganic Solids, Clarendon Press, Oxford, 1989.